Investigating the Fold and Absorption Efficiencies of PARIS

Oliver Roberts, Michał Ciemała

Dept. of Physics, Uni of York, Heslington, YO10 5DD, UK.
IFJ PAN, Kraków, Poland

May 2008

Abstract

This report summarizes the effects of Fold and Absorption efficiencies on a various array of different array and crystal sizes. It investigates a single module of detectors (known as the "Prototype") using a beam projected onto the surface. The effects and outcomes of the simulations for each scenario has been analysed and commented on . The work was then expanded further to include other simulations conducted with different amounts of segmentation and investigating the length of CsI. Other minor details were also touched upon and are explained in the following report in great detail. Further investigations are presented in order to expand what was discussed in this paper.

Introduction

In the first part of the report, I shall investigate the differing results from changing the parameters of the detectors used in the PARIS calorimeter, and how this changes the distribution of Fold, (the number of interactions confined to one crystal/detector).

I will also briefly touch upon the process involved when evaluating the simulated hits using the analyse files. In Geant4, one needs to construct an analyse file calibrated to what part of the detector/calorimeter one would wish to investigate. There are several versions of the calorimeter one can have, each with a different set-up and thus needing separate analyse codes to obtain the results. In the simulations investigating the fold distribution in the Prototype array, the central detector in the array was the detector checked relative to the other detectors around it. In the case of 3x3 segmentation of the Prototype wall, the central detector in a 3x3 array of detectors is the 5^{th} crystal. Further segmentation changes the position of this central detector, and thus in a 4x4 array, we have 4 potential central detectors; the 6^{th},7^{th},10^{th},11^{th} crystals. This is easy to do for just one wall, however to investigate this for an isotropic beamline incident on all 6 walls of the Pari scalorimeter, it becomes increasingly difficult. However, this is explained in more detail later on.

Simulated Work Involving Collimated Beamlines

The next few pages investigate which configuration is the best by using a collimated beam incident on one façade of the cubic geometry. For these simulations, the "Prototype" geometry was used, only the dimensions of the array and crystal sizes were changed. The fold was measured from the central detector (5^{th} crystal in 3 by 3 segmentation), and from that, we are able to see how many other detectors are affected for varying values of gamma.

As the dimensions of the crystal and array sizes change, the beam must be attenuated to compensate for this change. These changes are done in the set-up directory, in a basic generator text file where the dimensions of the collimated beam is given in spherical coordinates. Basic trigonometry is used to determine the parameters of the incident beamline, by measuring the values of θ and φ, which are

calculated by taking the length/height of the face, and dividing it by the source distance to the face of the $LaBr_3$ crystals. Then, taking the inverse tangent of this value to find α, one can deduce the parameters of the beam. In the case of an array of 2" crystals, 15cm from the source, one makes the following calculations:

```
.....# cascade: energy (in KeV) theta_min theta_max phi_min phi_max
              1000.              63          117         -27.        27.

#300.
#500.
#800....
```

Table 1: A portion of the beam generator code in the setup file "basic.gene" that shows the beam parameters for a 3x3 array of 2 inch crystals.

$\text{Tan}(\alpha)$ = height/ distance
$\alpha = \tan^{-1}(\text{height/distance}) = \tan^{-1}(15/15) = 27°$
Therefore, Start θ is: $90° - \alpha = 63°$
End θ: $180° - \alpha = 117°$
and both values of φ: $\pm \alpha = 27°$

For 2" crystals, a collimated beam in the positive x direction of multiplicity 7 was fired upon a 3 by 3 segmented arrangement of detectors, 15cm from the source. The gaps between the crystals was neglected (i.e. Set to zero) for this simulation as the consequent discrepancies associated with this will be discussed later. We observe the behaviour of fold with a collimated beam with a multiplicity of 7 ranging from 1 to 30MeV, increasing in steps of 5MeV.

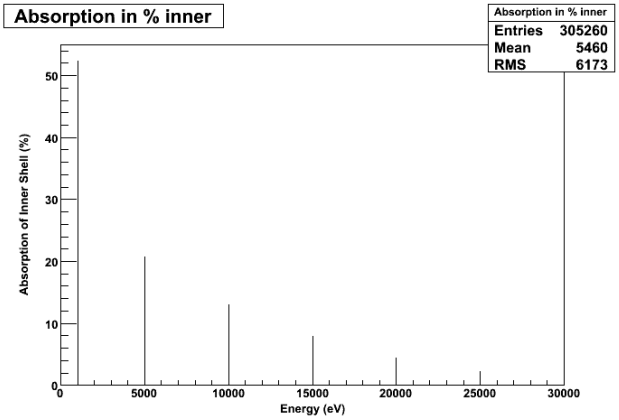

Illustration 1: The percent of absorption of 1,5,10,15,20,25,30MeV gammas in a 3x3 array of 2"x2"x2" $LaBr_3$ crystals.

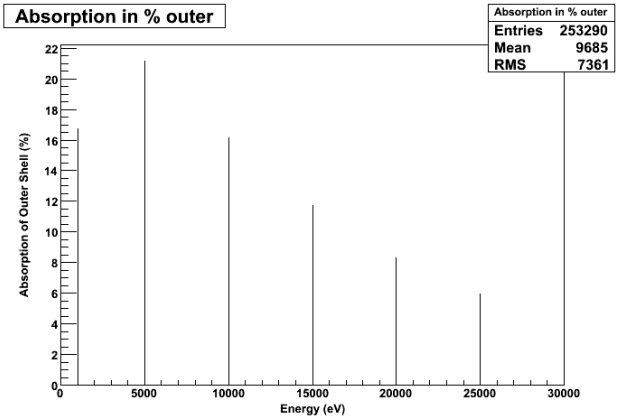

Illustration 2: The percent of absorption of 1,5,10,15,20,25,30MeV gammas in a 3x3 array of 2"x2"x6" CsI crystals.

After running 300,000 hits, the top two graphs (Illustrations 1 and 2), show the number of counts absorbed with varying incoming energy. We see that around ~52% of incoming gammas with incident energy 1MeV are absorbed in the inner shell of $LaBr_3$ crystals, while only ~17% are absorbed in the outer shell of CsI crystals. One notes that the trend of the absorption in the inner $LaBr_3$ crystals is decreasing with increasing energy. This can be expected as the energy of high energy gammarays can not be confined to such a volume of space. The pattern with absorption in the outer CsI crystals is different as one observes a "peak" in absorption, where ~21% of 5MeV gammas are contained within the detectors.

Looking at the relevant Fold graphs, starting with the fold in the inner shell of crystals, we see that

only the central detector is really effectedat low gamma energies, however we see the majority of interactions in 1 fold changeover to 2 fold after around 10MeV. This majority remains the same, peaking at 30MeV in this simulation. This increase in 2 fold is accompanied by a similar increase in folds 3 and 4, although not of the same magnitude.

For the fold in the outer shell of CsI crystals we observe a similar trend; an increase in energy is proportional to the number of detectors that detect reactions in the wall. At low energies, most of the interactions were confined, again to 1 fold, until the majority switches over to 2 fold at around 5-10MeV. The number of interactions in 2 fold is steady, quite linear, and seems to plateau out at high energies. This is different to the remaining folds, as rise of interactions in 3 fold peaks at roughly the same point as the number of detections in 2 fold, after following a rapid increase in the number of detections with increasing energy.

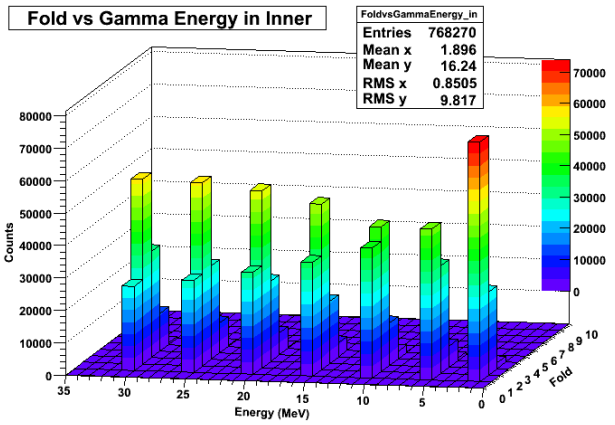

Illustration 3: Fold distribution for individual detectors centred around the middle detector with incident 1,5,10,15,20,25,30MeV gammas in a 3x3 array of 2"x2"x2" $LaBr_3$ crystals

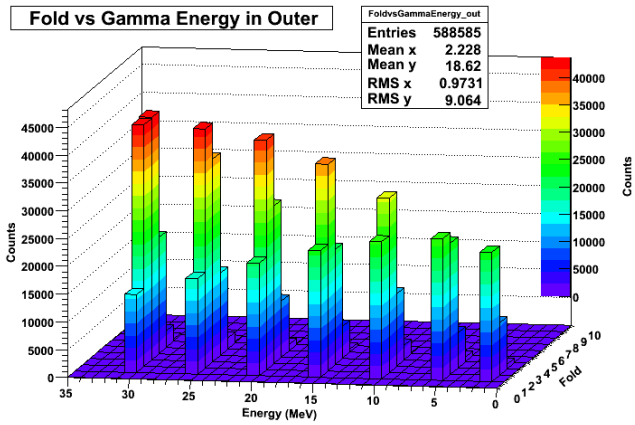

Illustration 4: Fold distribution for individual detectors centred around the middle detector with incident 1,5,10,15,20,25,30MeV gammas in a 3x3 array of 2"x2"x6" CsI crystals

Overall, it appears to confirm what one would expect, and increase in the energy of the incident gammas, means an increase in the number of fold, but how does this compare when we increase the size of the crystals? Increasing the size of the crystal would mean more interactions would be contained within this volume, and thus one would see more absorption and less fold as more energy would become deposited in fewer detectors. Taking this into account, we now observe what happens when the array size is kept fixed and the crystal size is increased from 2" to 3".

The first thing one notices is the change in efficiencies. There is an increase in the absorption efficiency of inner crystals due to an increase in the volume, which in turn means more interactions can be allocated to these crystals and read out. However, the efficiency with regards to the amount of absorption in the outer shell of CsI crystals is lower. This poorer efficiency is due to the increased source distance, meaning more interactions are likely to be contained within the $LaBr_3$ crystals. Therefore, we see a peak in absorption at ~70% for 1MeV gammas in inner crystals, and ~14% for 5MeV gammas in the outer shell.

Looking at the Fold graphs for the inner detectors, we observe a similar trend; for energies lower than 10MeV, the probability for the number of interactions to be allocated within one fold is very high. This dominance changes at around 10-15MeV where the majority of interactions are confined to 2 fold, which happens at a higher energy than the previous fold graph for these crystals.

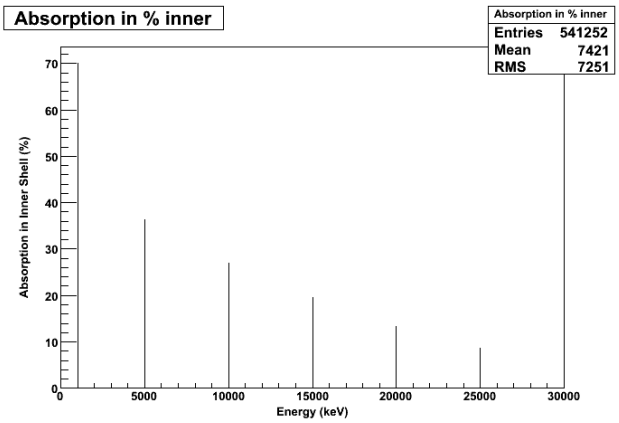

Illustration 5: The percent of absorption of 1,5,10,15,20,25,30MeV gammas in a 3x3 array of 3"x3"x3" $LaBr_3$ crystals.

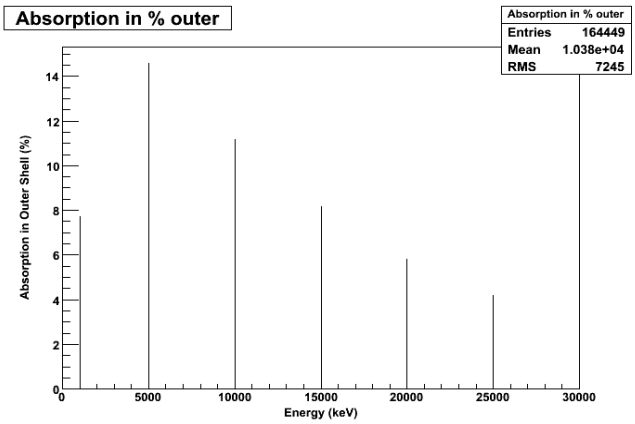

Illustration 6: The percent of absorption of 1,5,10,15,20,25,30MeV gammas in a 3x3 array of 3"x3"x6" CsI crystals.

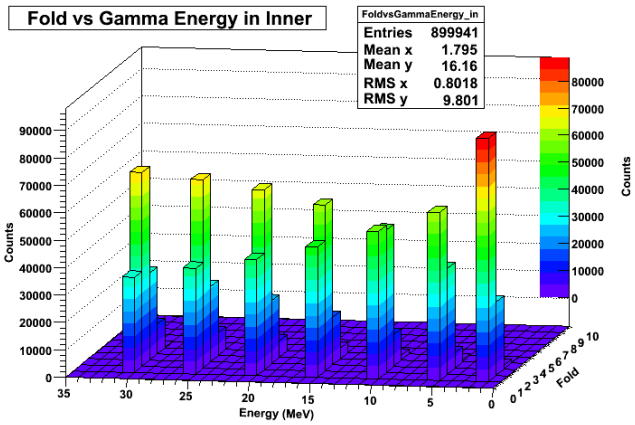

Illustration 7: Fold distribution for individual detectors centred around the middle detector with incident 1,5,10,15,20,25,30MeV gammas in a 3x3 array of 3"x3"x3" $LaBr_3$ crystals

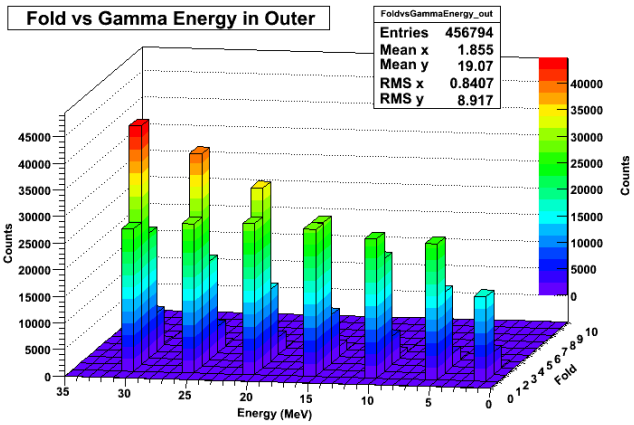

Illustration 8: Fold distribution for individual detectors centred around the middle detector with incident 1,5,10,15,20,25,30MeV gammas in a 3x3 array of 3"x3"x6" CsI crystals

In the graph representing the fold nature for the outer shell of crystals, the trends are roughly the same, although the efficiency is diminished somewhat. The number of detectors that showed a deposit of energy with regard to the central detector increases dramatically after 1MeV, where most of these interactions are confined to the inner shell and do not possess enough energy to travel to the outer shell. The nature of 1 fold is relatively flat nature with a peak of about 20MeV. There is an increase in the number of detections in 2 fold, peaking at high energies (highest here being 30MeV).

I would like to remind the reader that although we are just dealing with one wall of the tiled PARIS calorimeter, the distance from the wall to the source were kept at a distance by which one can tile the detector without hindrance, into a 4π cubic array. The source distance for the 3x3 segmented array of 2" $LaBr_3$ crystals was 15cm and for the CsI was 20cm. For the case of 3" crystals in a 3x3 array, the source distance to the inner $LaBr_3$ crystals was 22.5cm and 30cm to the outer CsI crystals. Finally, the source distance in the case of a 3x3 array of 4" $LaBr_3$ crystals was 30cm and 40cm to the face of the CsI crystals in the same configuration.

Taking this into account, we now examine the final fold graph using 4" crystals in a 3x3 array. We keep the same parameters as all the other measurements and obtain the following.

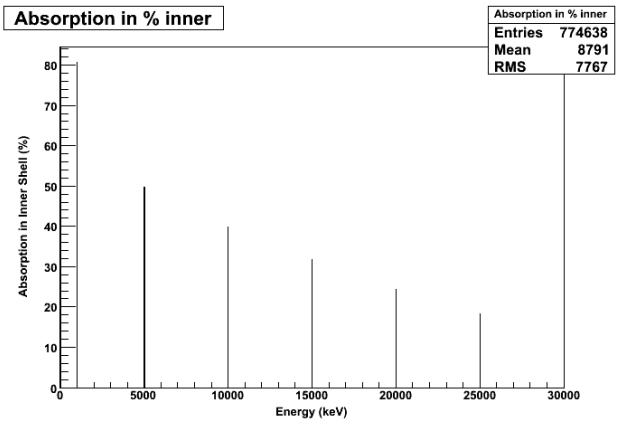

Illustration 9: The percent of absorption of 1,5,10,15,20,25,30MeV gammas in a 3x3 array of 4"x4"x4" $LaBr_3$ crystals.

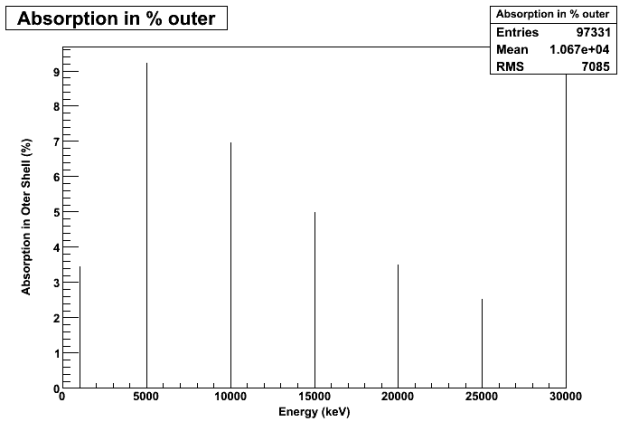

Illustration 10: The percent of absorption of 1,5,10,15,20,25,30MeV gammas in a 3x3 array of 4"x4"x6"CsI crystals.

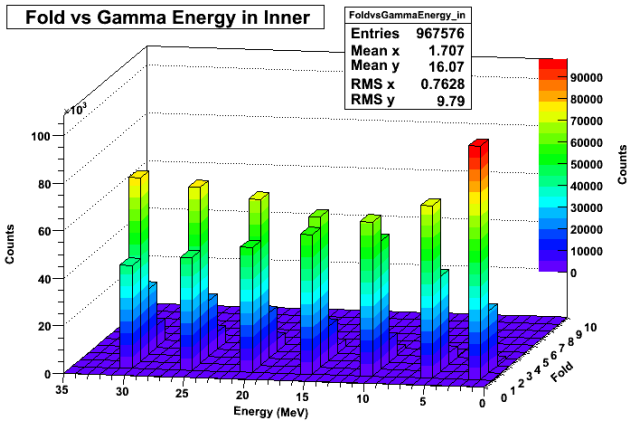

Illustration 11: Fold distribution for individual detectors centred around the middle detector with incident 1,5,10,15,20,25,30MeV gammas in a 3x3 array of 4"x4"x4" $LaBr_3$ crystals

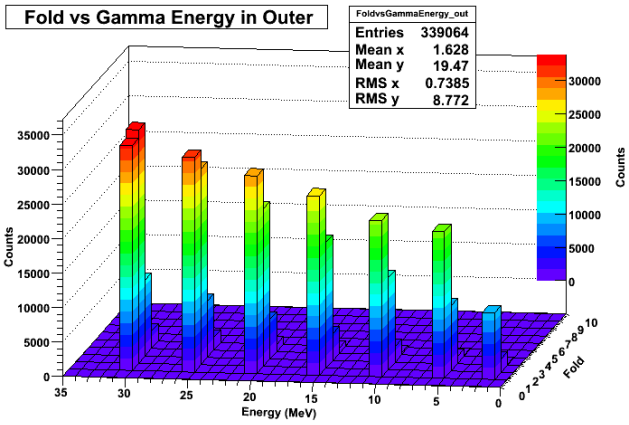

Illustration 12: Fold distribution for individual detectors centred around the middle detector with incident 1,5,10,15,20,25,30MeV gammas in a 3x3 array of 4"x4"x6" CsI crystals

For 4" crystals in a 3x3 array, one can determine that the efficiency of the inner crystals is greater than the outer crystals. This is apparent if we study the absorption graphs above. Around 80% of 1MeV gammas are absorbed in the $LaBr_3$ crystals, and even high energy gammas(>15MeV) have a high amount of absorption 15-25% in the inner shell of detectors compared to the outer shell where there is a peak absorption efficiency of ~9% for 5MeV gammas.

These trends are reflected in the relating Fold graphs. In the inner shell, there is a large number of counts associated with just one fold at 1MeV, but this trend declines, and the point where 2 fold readouts occur is at around 10-15MeV. 2 Fold interactions peak at high energy incident gamma rays, in my simulation, at 30MeV. For the Fold distribution in the outer shell of CsI crystals, One notices that the majority of interactions held within just one fold dominates up to around 30MeV, where there is a peak in the readout of 2 fold interactions. There are also very few reactions contained in any fold at 1MeV due to the high absorption rates in the inner shell. To conclude, we also see the number of hits in the outer shell drop with increase in crystal size, due to the increasing source distance, this is not as much of a problem with the $LaBr_3$ crystals as more gammas are incident and contained within such a large volume.

Now we must ask, do we observe similar trends when we do something similar for an increased array size of 4x4 crystals? Does a larger array necessarily make it better due to a large collection area despite greater distances from the incident planes of the crystals to the source? The last set of fold

graphs was the amount of fold relative to the central detector in a3x3 arrangement (the 5th detector, where a beamline would probably be added). Now, I am going to investigate a 4x4 arrangement, where there is not 1 central detector, but where the centre of the face exists at the corner of 4 detectors. One can assume that there will be negligible differences between these detectors, and that all should roughly be the same. Simulations were conducted to verify this just in case. The outstanding detector from these simulations that proved to be the best would then be used in subsequent simulations where the crystal sizes changed.

First, the analyse files had to be changed from analysing a 3x3 array of detectors, relative to the central detector, to our new scenario of 4x4 crystals. I ran a simulation of 300,000 incident gammas and investigated which central crystals had the best fold distribution. The central crystals are the 6th, 7th, 10th and 11th crystals, arranged in a fashion similar to the diagrams below due to a loop in the analyse file on how the data is read.

```
// for (Int_t j=1; j<7;j++) { // for six walls
for (Int_t k=0;k<4;k++){
                for(Int_t l=1; l<=4;l++){
                edepsum_inner[i]+=fcRootEv->SummEnergyInDet(i,10000+k*4+l);
                        if((fcRootEv->SummEnergyInDet(i,10000+k*4+l)))
                            temp_fi++;
                 }
        }
```

Table 2: The nested loop in the analyse code showing how the data is read

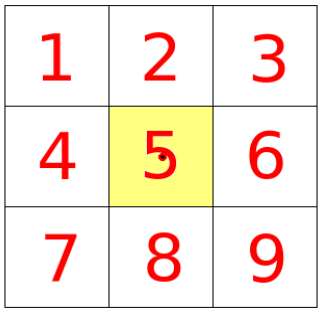

Illustration 1: An illustration showing the central detector (shaded) in a 3x3 detector array.

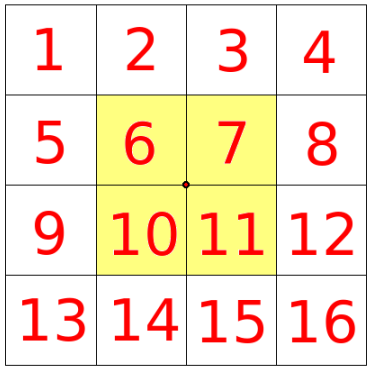

Illustration 2: An illustration showing the central detectors(shaded) in a 4x4 detector array.

With this in mind, I obtained the following graphs below and found that the absorption is the same in all 4 absorption graphs, although there are very slight differences in the number of events in the fold graphs. In the absorption graphs, for a 2" crystal in a 4x4 array, all four central crystals showed a peak of ~54% for incident gammas of 1MeV. This quickly dropped off with increasing energy, with only >10% of 15MeV gammas being absorbed in the inner shell of crystals. In the absorption of gammas in the outer shell of crystals, ~24% of incident 5MeV gammas are absorbed. The other absorption rates are lower, and in some cases are lower then the absorption in the inner shell of crystals at the same energy, especially at high energies.

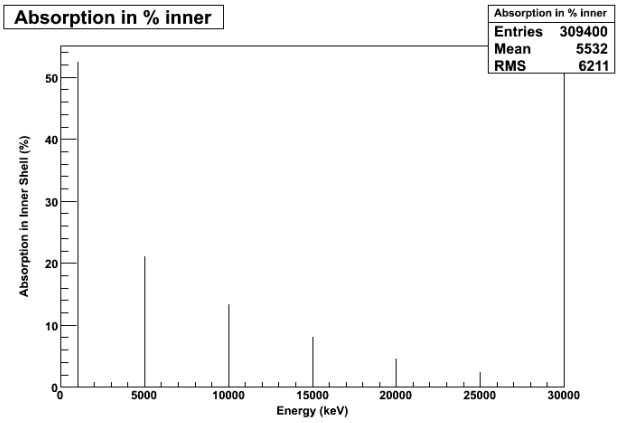

Illustration 13: The percent of absorption of 1,5,10,15,20,25,30MeV gammas in central detectors 6,7,10,11 in a 4x4 array of 2"x2"x2" $LaBr_3$ crystals.

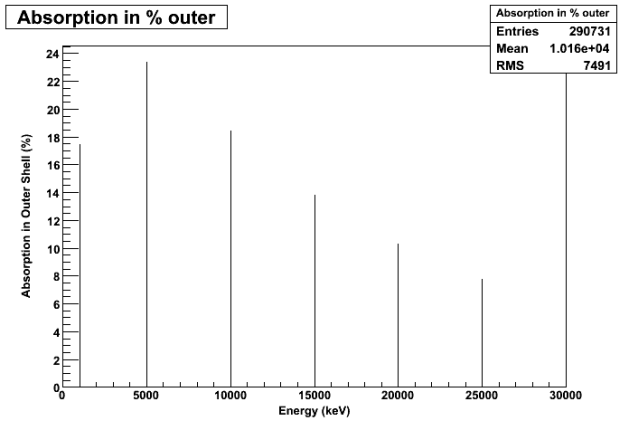

Illustration 14: The percent of absorption of 1,5,10,15,20,25,30MeV gammas in central detectors 6,7,10,11 in a 4x4 array of 2"x2"x6" CsI crystals.

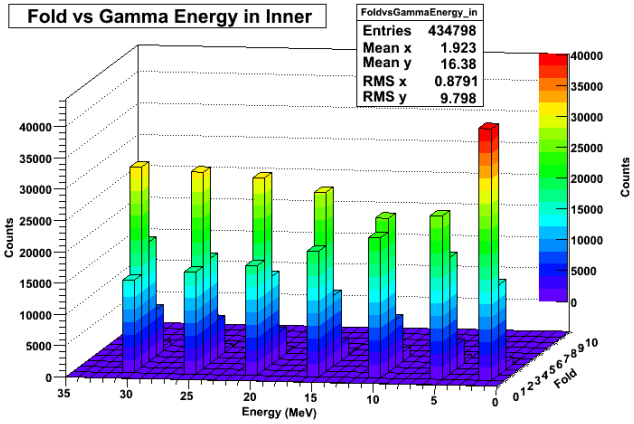

Illustration 15: Fold distribution for the central 6th detectors with incident 1,5,10,15,20,25,30MeV gammas in a 4x4 array of 2"x2"x2" $LaBr_3$ crystals

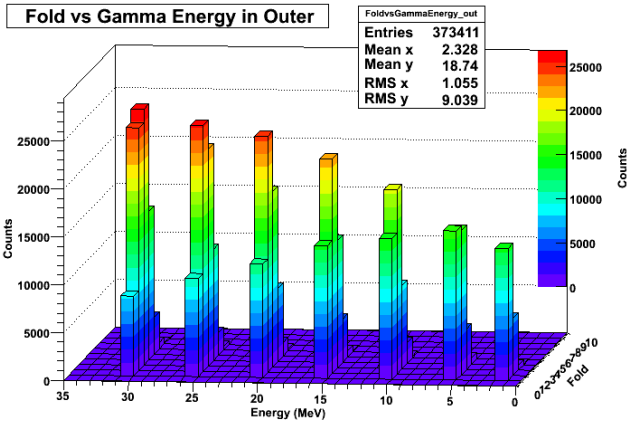

Illustration 16: Fold distribution for the central 6th detector with incident 1,5,10,15,20,25,30MeV gammas in a 4x4 array of 2"x2"x6" CsI crystals

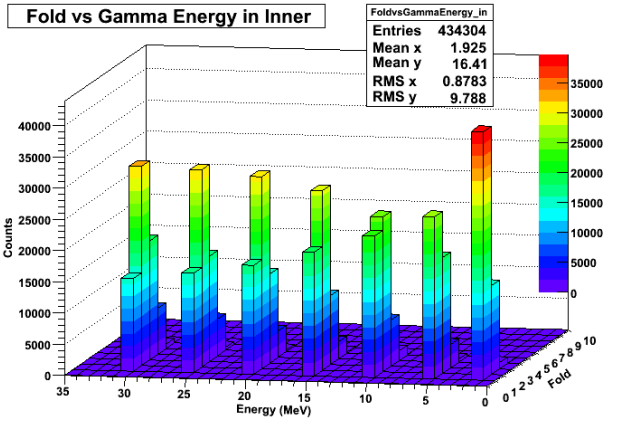

Illustration 17: Fold distribution for the central 7th detector with incident 1,5,10,15,20,25,30MeV gammas in a 4x4 array of 2"x2"x2" $LaBr_3$ crystals

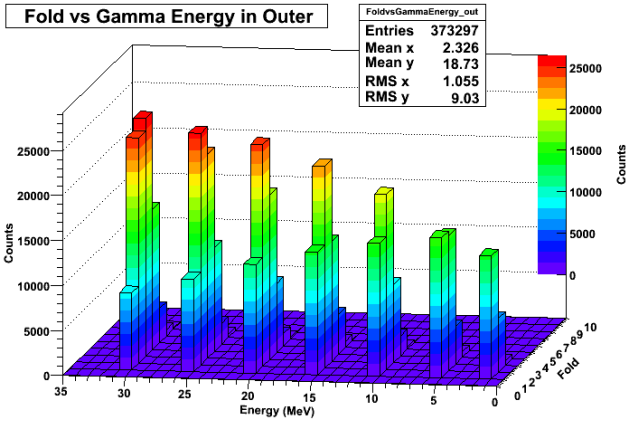

Illustration 18: Fold distribution for the central 7th detector with incident 1,5,10,15,20,25,30MeV gammas in a 4x4 array of 2"x2"x6" CsI crystals

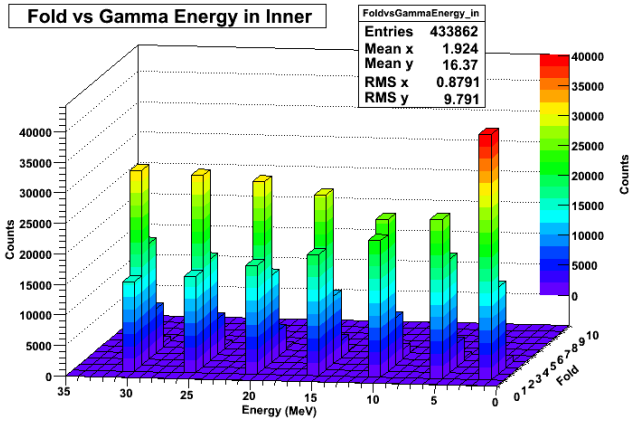

Illustration 19: Fold distribution for the central 10th detector with incident 1,5,10,15,20,25,30MeV gammas in a 4x4 array of 2"x2"x2" $LaBr_3$ crystals

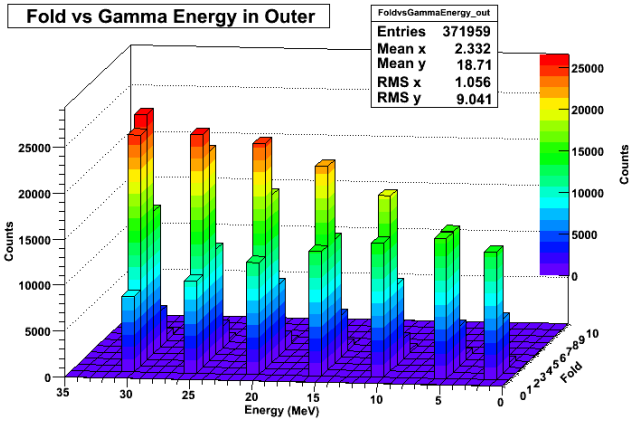

Illustration 20: Fold distribution for the central 10th detector with incident 1,5,10,15,20,25,30MeV gammas in a 4x4 array of 2"x2"x6" CsI crystals

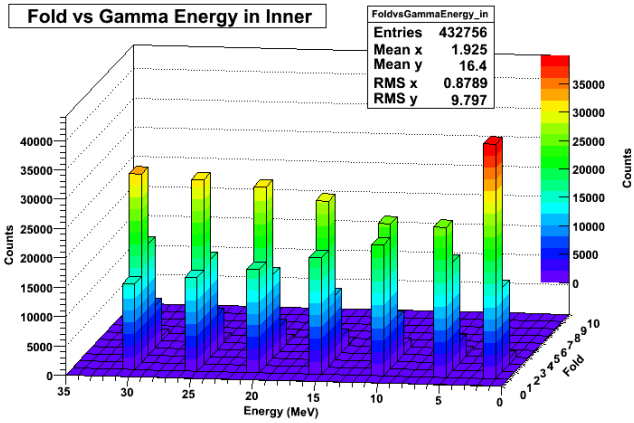

Illustration 21: Fold distribution for the central 11th detector with incident 1,5,10,15,20,25,30MeV gammas in a 4x4 array of 2"x2"x2" $LaBr_3$ crystals

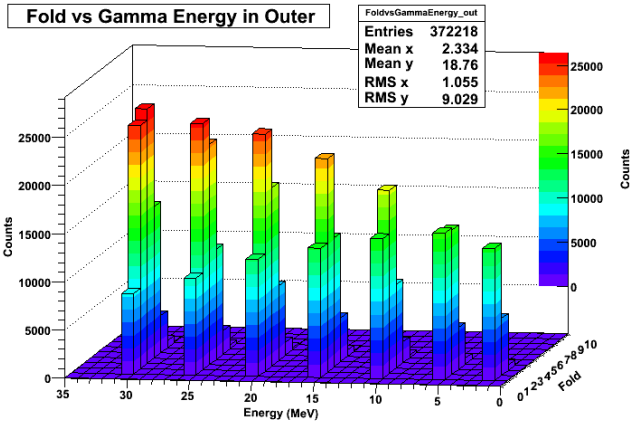

Illustration 22: Fold distribution for the central 11th detector with incident 1,5,10,15,20,25,30MeV gammas in a 4x4 array of 2"x2"x6" CsI crystals

As mentioned previously, there is a very slight difference between the different fold counts, although the trends in each are identical. To be consistent, the same output file with the number of runs was used, the analyse file was just tweaked so that it would read the 6th ,7th ,10th and 11th detectors respectively. Looking at the fold histograms, the greatest number of registered counts were in the 6th and 7th detectors, with the 6th detector having the most. This result is true for both inner and outer detectors, and the trends for each are almost identical. Therefore, it is safe to assume that the 6th detector will provide us with the best results for the next two simulations where I made the crystal volume bigger by increasing its size, as was the case with the previous simulations involving a 3x3 array. Keeping the parameter the same, but increasing the crystal size by an inch, and then 2 inches, one obtains the following absorption and fold graphs for 3" and 4" crystals.

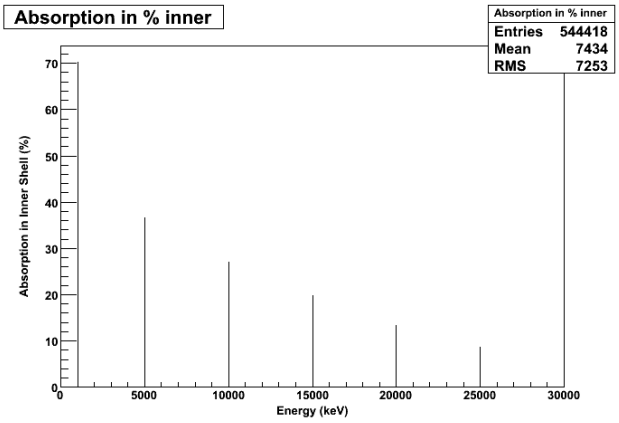

Illustration 23: The percent of absorption of 1,5,10,15,20,25,30MeV gammas in the central 6th detector in a 4x4 array of 3"x3"x3" $LaBr_3$ crystals.

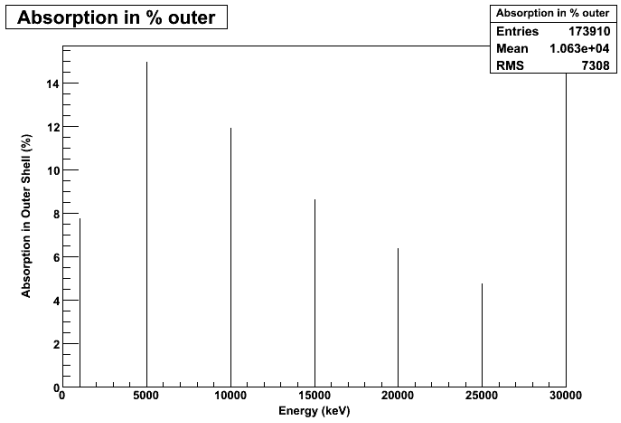

Illustration 24: The percent of absorption of 1,5,10,15,20,25,30MeV gammas in the central 6th detector in a 4x4 array of 3"x3"x6" CsI crystals.

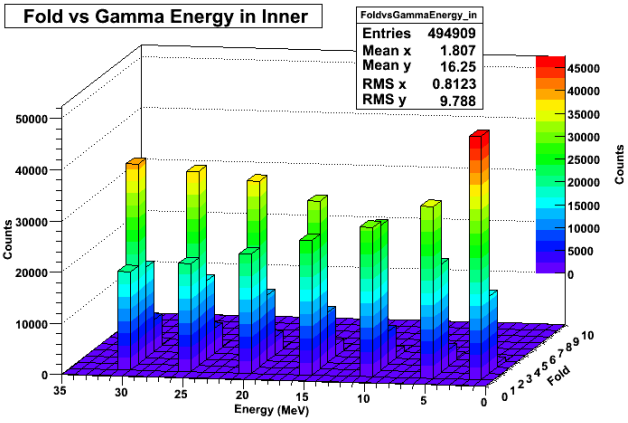

Illustration 25: Fold distribution for the central 6th detector with incident 1,5,10,15,20,25,30MeV gammas in a 4x4 array of 3"x3"x3" $LaBr_3$ crystals

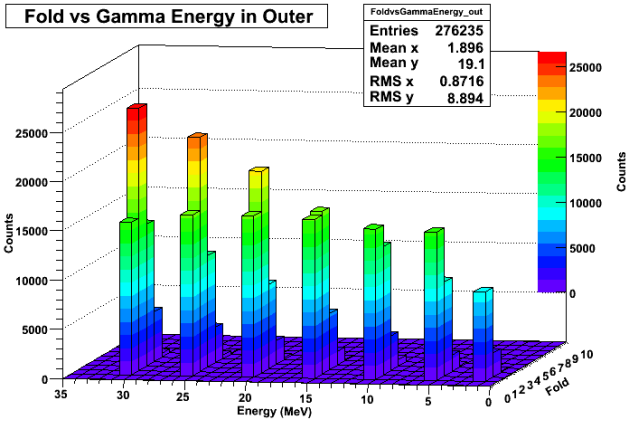

Illustration 26: Fold distribution for the central 6th detector with incident 1,5,10,15,20,25,30MeV gammas in a 4x4 array of 3"x3"x6" CsI crystals

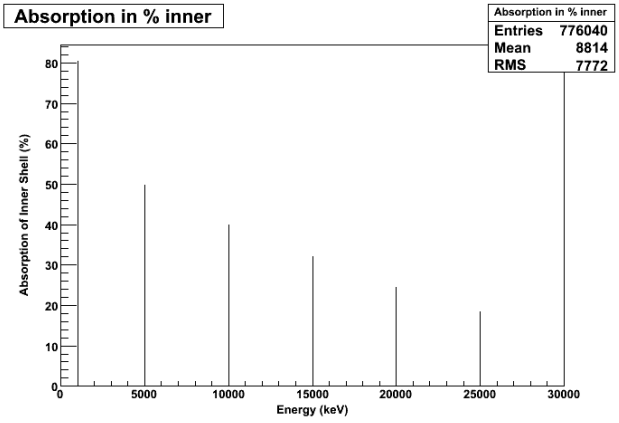

Illustration 27: The percent of absorption of 1,5,10,15,20,25,30MeV gammas in the central 6th detector in a 4x4 array of 4"x4"x4" $LaBr_3$ crystals.

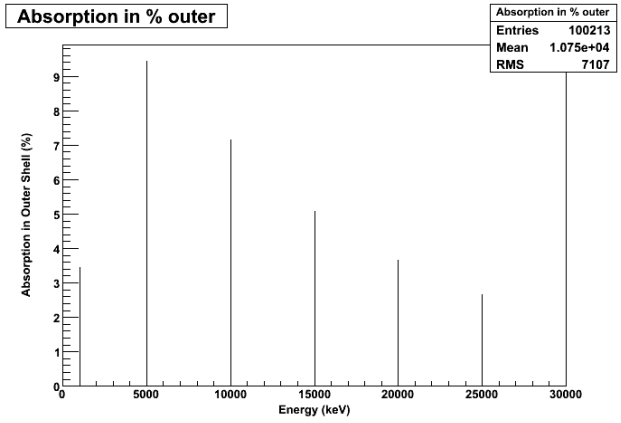

Illustration 28: The percent of absorption of 1,5,10,15,20,25,30MeV gammas in the central 6th detector in a 4x4 array of 4"x4"x6" CsI crystals.

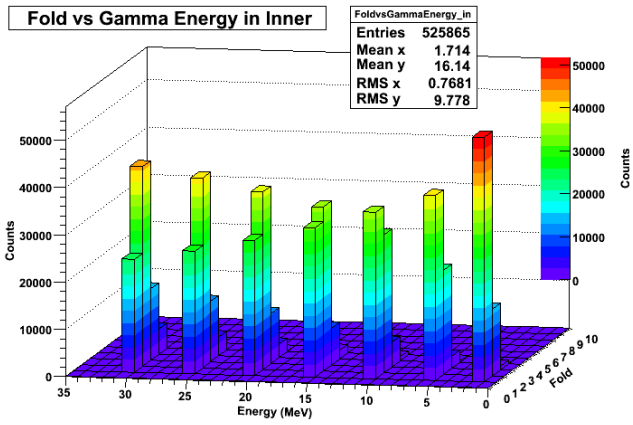

Illustration 29: Fold distribution for the central 6th detector with incident 1,5,10,15,20,25,30MeV gammas in a 4x4 array of 4"x4"x4" $LaBr_3$ crystals

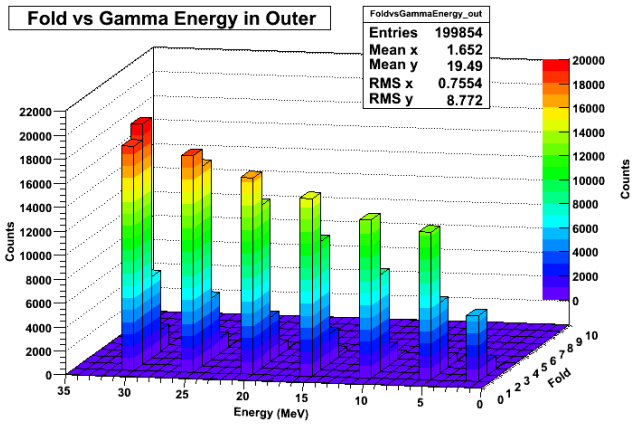

Illustration 30: Fold distribution for the central 6th detector with incident 1,5,10,15,20,25,30MeV gammas in a 4x4 array of 4"x4"x6" CsI crystals

After running the simulation for a 4x4 array of 3" and 4" crystals using the "Prototype" arrangement, we see similar trends in these graphs when comparing them to earlier graphs, starting first with the absorption graphs. In the case of absorption trends for a 4x4 array of 3" crystals, we see a peak in the absorption of ~70% for incident 1MeV gammas for the inner shell and a peak of ~14% for incident 5Mev gammas in the outer shell. These results are consistent, and almost identical to similar sized crystals in the 3x3 arrangement, the only real difference being that the number of counts is fractionally bigger in the 4x4 arrangement, as one might expect. Similarly, for the larger 4" crystals, the absorption rates are the same as those in a 3x3 arrangement, with only slight discrepancies in the amount of absorption. Again, however, the number of counts for the larger crystals was fractionaly larger, but the amount really can be negligible.

Looking now at the fold graphs, we have a bit more to talk about. In the case of the 3" crystals in the 4x4 array, the number of counts are almost half of what was observed in the case of the same sized crystals in the 3x3 arrangement. This shows that the increased distance from the source distance plays a crucial role in the efficiency of these crystals. The trends in the graphs are similar to previous simulations, with the number of fold only shifting slightly. In the inner shell, we see a peak of 1 fold for low energy gammas, and that this dominance does not change until around 10MeV where 2 fold majority dominates, and then peaks at 30MeV. There is a slight decrease in the number of interactions held within the 4^{th} and 5^{th} folds, which is what one might expect there to be due to the large volume of crystal. For the outer shell of 3" crystals, the trends are noticeably different, the number of 3 fold or one fold interactions is significantly less than either the 2" or 4" graphs involving the same array size and simulations. This is a result of increasing crystal size. For the 2" simulation, there was a high number of interactions in the 2^{nd} and 3^{rd} folds, and by the time we simulate the same scenario involving 4" crystals, we find hardly any interactions held in the 3^{rd} fold, however, the majority of energy deposited is allocated to the 1^{st} and 2^{nd} folds. As a result, there is only a 2-fold peak at 30MeV, but two fold interactions have the dominate majority from around 15MeV onwards. Previous to this turnover point, 1 fold holds the majority of interactions, which is what one might expect for low energy gammas. With the inner shell of 4" crystals, there are similar trends to the previous graphs, with a peak in 1 fold interactions at low energies, and a peak in two fold interactions for 30MeV gammas. In the outer shell, more interactions are held within the 1^{st} and 2^{nd} folds, and this is still the case even at high energies, with the amount of energy being deposited in the "lesser" folds (ie. >3) being very small.

The overall trend can now be seen in the following 5 graphs which show the absorption efficiencies for different crystal sizes, in different arrays and with different incident energies.

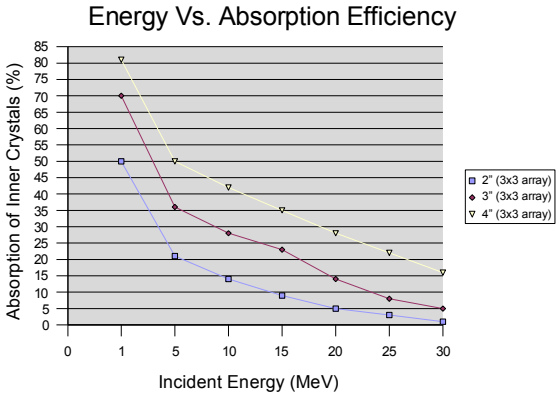

Illustration 31: A graph to show the incident energy plotted against absorptionefficiency for $LaBr_3$ crystals in a 3x3 array

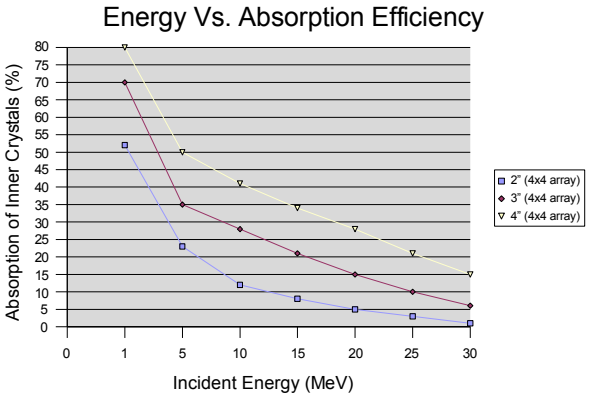

Illustration 32: A graph to show the incident energy plotted against absorptionefficiency for $LaBr_3$ crystals in a 4x4 array

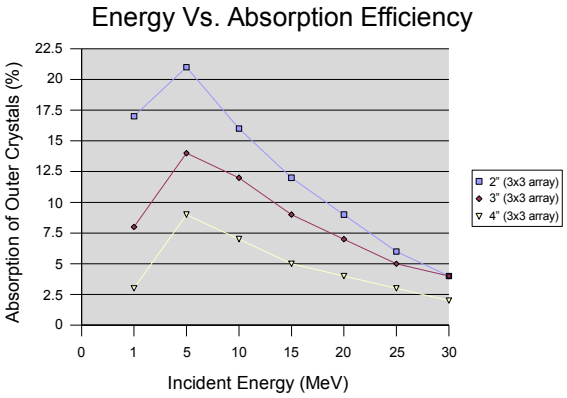

Illustration 33: A graph to show the incident energy plotted against absorption efficiency for CsI crystals in a 3x3 array

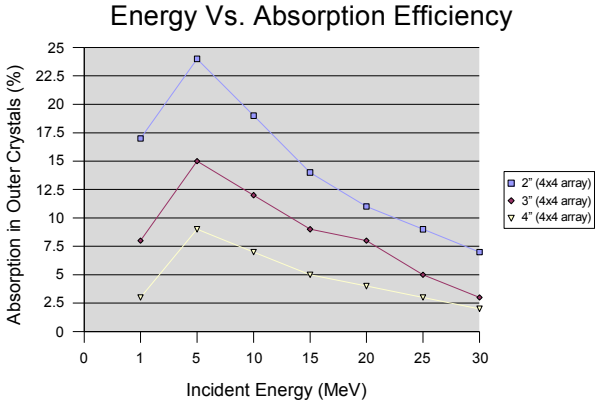

Illustration 34: A graph to show the incident energy plotted against absorption efficiency for CsI crystals in a 4x4 array

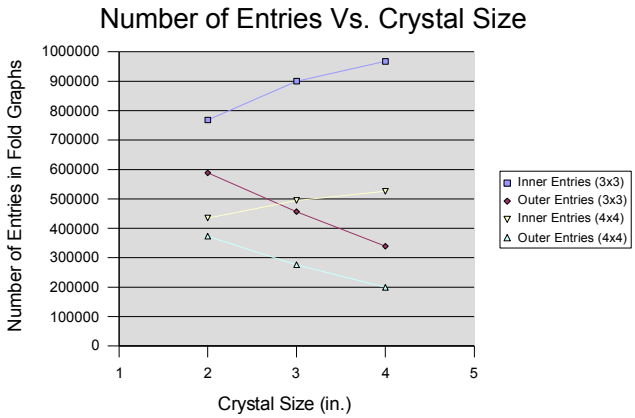

Illustration 35: A graph to show the number of entries plotted against the increasing crystal size for 3x3 and 4x4 arrays, taking off the fold graphs

Now, one can move on to look at moreexotic possibilities of segmentation that could better or worse the results, and this shall be investigated intensely in the following section.

Effects of a Collimated, High Multiplicity Beam on Segmented Arrays.

Next, we can apply what we have done to the case of the "Prototype", to a new façade which involves further segmentation of both CsI and $LaBr_3$ crystals in both shells. This is still done with the old prototype geometry in the set-up directory, in the following way.

```
# where front mean: +x axis
# All dimensions in cm
# cube_name material  DetNumPerOne Width_wall(front)  Dist_src_wall  Length_wall
Thick_wall      Hole_segm       active
Inner     LaBr3       3                   30.0        30.0        10.0        0           1
Outer     CsI         6                   40.0        30.0        15.0        0           1
#
```

Table 3: This is the code needed to perform the segmented prototype simulations, in this case a 3x3 array for 4" $LaBr_3$ and 2" CsI crystals respectively.

A 3x3 array was only used as arrays larger than this would show great inefficiency due to the growing source distance to accommodate for the cubic geometric configuration.

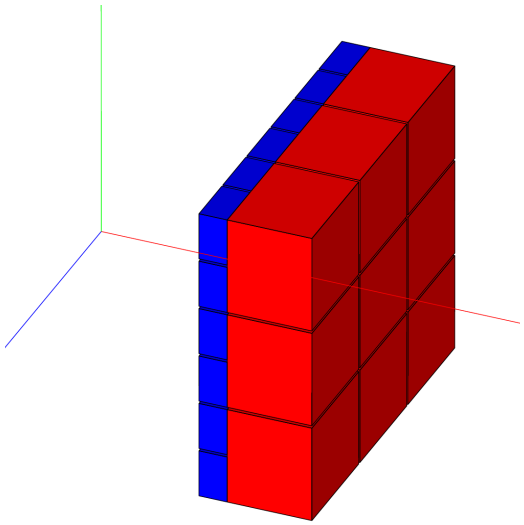

Illustration 36: This shows the segmented inner 2" $LaBr_3$ crystals (Blue) and 4" CsI crystals (Red), length of which was fixed at 6" in a 3x3 array.

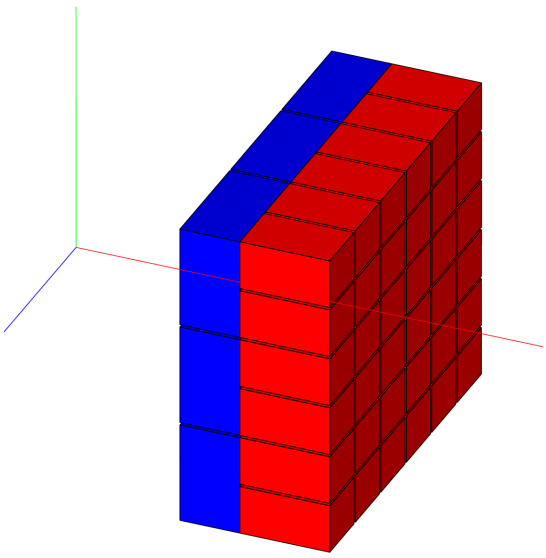

Illustration 37: This shows the segmented inner4" $LaBr_3$ crystals (Blue) and 2" CsI crystals (Red), length of which was fixed at 6" in a 3x3 array.

Looking at these two different segmented arrays, one can predict that the segmented surface will experience a massive drop in the number of counts compared to previously simulated arrays. Again, the distance from the source was simulated as if the wall was tiled, this is to ensure we have consistent sets of data. The gaps were changed to 5mm (we will later understand that this is the best value for this parameter later), and an incident energy beam had the energy ranges 1,5,10,15,20,25, and 30MeV.

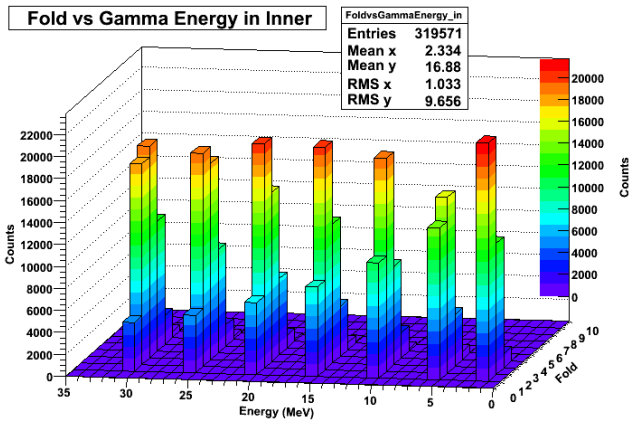

Illustration 38: Fold graph to show the effects of counts in the number of fold at different values of incident energies for 2" $LaBr_3$ crystals in a 6x6 arrangement, 30cm from the source.

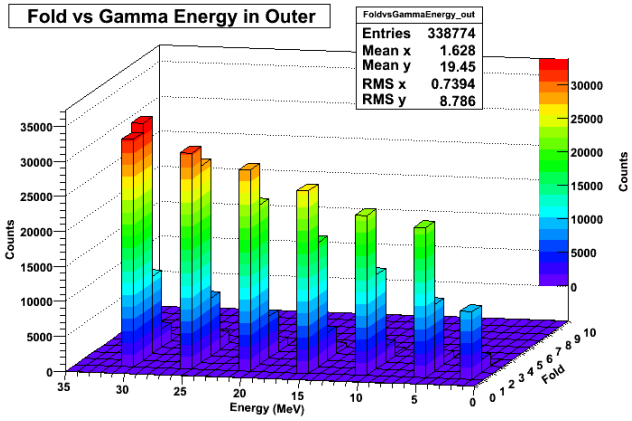

Illustration 39: Fold graph to show the effects of counts in the number of fold at different values of incident energies for 4" CsI crystals in a 3x3 arrangement, 40cm from the source.

Here we have the inner shell of $LaBr_3$ crystals segmented further and observe a very poor efficiency in terms of number of interactions. However, the fold distribution is strikingly different in the sense that the number of folds is much greater than for any other previous graph. There is a peak in 1 fold at 1MeV, which one might expect, however, there is no longer a peak for two fold interactions! At 30MeV, most of the majority of incident gammas deposit their energy in three fold, with two fold interactions peaking at around 20MeV. We expect the outer shell of crystals to behave, and have values similar to, the fold graph for 4" in a 3x3 array in the previous simulation, and this holds true.

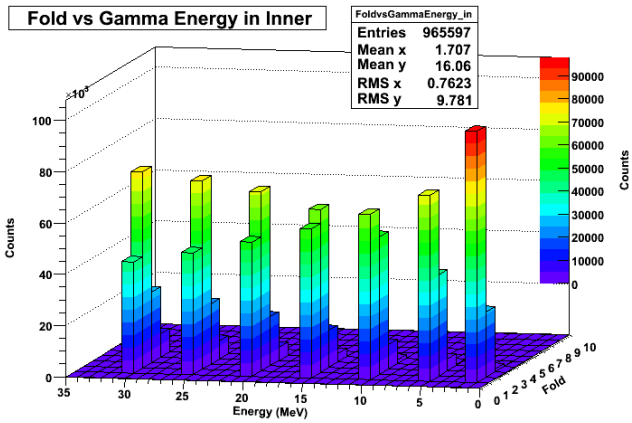

Illustration 40: Fold graph to show the effects of counts in the number of fold at different values of incident energies for 4" $LaBr_3$ crystals in a 3x3 arrangement, 30cm from the source.

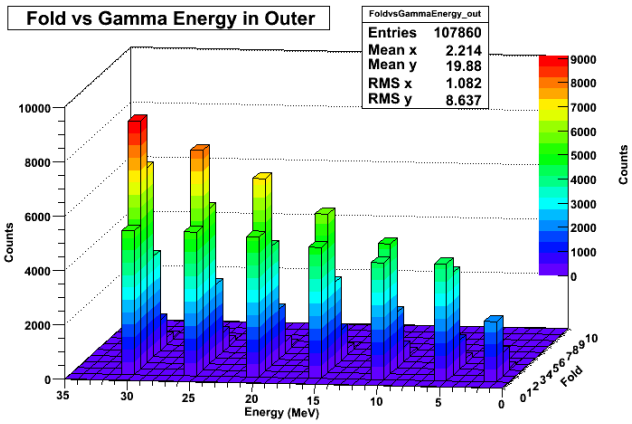

Illustration 41: Fold graph to show the distribution of counts in the number of fold at different values of incident energies for 2" CsI crystals in a 6x6 arrangement, 40cm from the source.

If we reverse what we did for the first set of graphs and segment the outer shell of CsI crystals, we obtain the fold graphs above. The inner shell of crystals are expected to have trends and values identical to previous simulations investigating that arrangement, and this case is no exception. However, the segmented outer shell of crystals show a poor number of counts, and a low number of interactions incident on the detectors. In this simulation, detector 16 was chosen as it is closest to the centre of the detector, in a much similar problem to what was discussed with the 4x4 arrangement. Taking this into account, we see a majority of interactions above 15MeV are held in the first 3 folds, with an increasing amount of energy being deposited in the 4^{th} and 5^{th} folds at 30MeV, although the peak here is 2 fold. There is little activity for low energy gammas in this shell due to the dominating role a large volume in the inner shell has in containing most of the gammas at this energy.

Looking at the graphs above, it is safe to assume that further segmentation of either the $LaBr_3$ or CsI crystals in the manner described yields poor results. The source distance also becomes a contributing factor when dealing with the case where the CsI crystals are segmented. I would hypothesize that lowering the size of both the array and crystal would allow us to obtain more counts, however it would sacrifice a better fold distribution. With this in mind, I conclude that the best arrangement to use would either be a 4x4 array of 2" crystals or a 4x4 array of 3" crystals. If one wanted to maximize the count rate in the inner detector and wasn't too concerned with the consequent effect this would have on the outer shell, then the 4x4 array of 3" crystals would be the best choice. However, if one was concerned with both the efficiency of both the inner and outer shells of detectors, the arrangement of 2" crystals in a 4x4 array would be the best configuration to use. Here, I will use the latter in further experimentation from this point on as it's properties are most beneficial to PARIS.

The Effects of Other Parameters on the Count and Fold Distribution

The Length of CsI used.

Up until now, the length of the outer shell of CsI crystals have stayed fixed at 6". However, it is interesting to see if any increase in this length would yield a substantial higher count rate. If this was true, then one could extend the outer shell of CsI crystals to compensate for the source distance when large, efficient $LaBr_3$ crystals are used. First, I will simulate a wall using the best array found from the previous chapter, with a beamline of several multiplicities, and will then examine the effect this increase in length has on the number of counts.

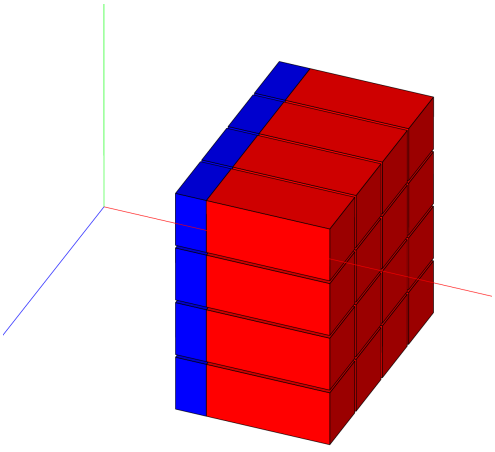

Illustration 42: This shows the configuration of a 4x4 array of 2" crystals with the length of CsI crystals(Red) extended to 8" in length.

First, the length of CsI crystals was extended 2" from previous measurements of 6" to 8". The first simulation was conducted at a number of incident energies similar in size to what was used in previous simulations.

The inner shell of $LaBr_3$ crystals are 20cm from the source, this is so that in the case when they are tiled, there are no overlapping volumes. The outer CsI crystals are 25cm from the source, implying a size of 2"x2"x2" for the $LaBr_3$ crystals and 2"x2"x8" for the CsI crystals. The array was tested with incident energies of 1,5,10,15,20,25, and 30MeV. One would expect a similar fold distribution for the inner shell of crystals to previous simulations at that particular size. However, we expect an increase in the number of counts for CsI crystal due to its volume extension.

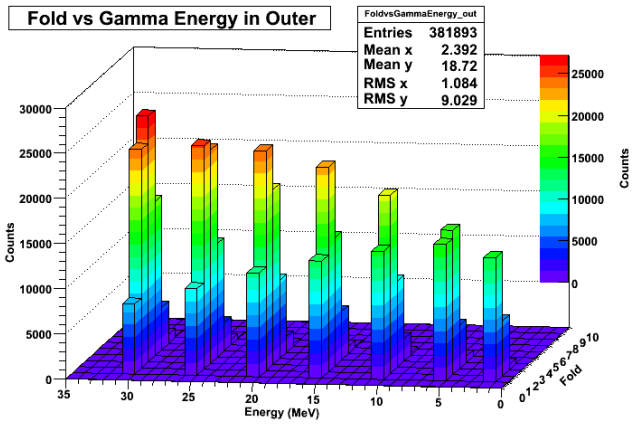

Illustration 43: Fold distribution for the central 6th detector with incident 1,5,10,15,20,25,30 MeV gammas in a 4x4 array of 2"x2"x8" CsI crystals

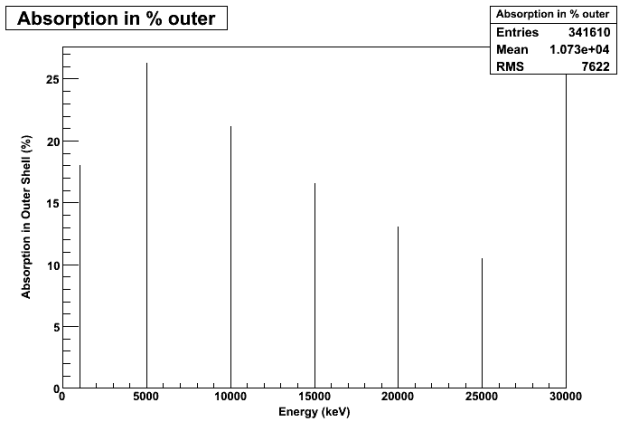

Illustration 44: The percent of absorption of 1,5,10,15,20,25,30 MeV gammas in the central 6th detector in a 4x4 array of 2"x2"x8" CsI crystals.

Looking at the graphs, the trend in the fold distribution is the same for the similar simulation and consequent fold graph, although one does note a rise of ~2.2% in the number of counts, and increase in absorption. Although, this was predicted, it is only a small increase. At the end of the previous section, I defined two possible configurations for which one can choose to better the outcome of their experiment. Having tried the 2" crystals in a 4x4 arrangement, I thought it would be interesting to see if the other configuration (3" crystals in a 4x4 array) yielded similar results, or if they were better. Would extending the length be enough to compensate for the increased source distance? If this is the case, then this configuration would be more favoured over the one on which we agreed upon due to its higher absorption rates in the inner shell of crystals.

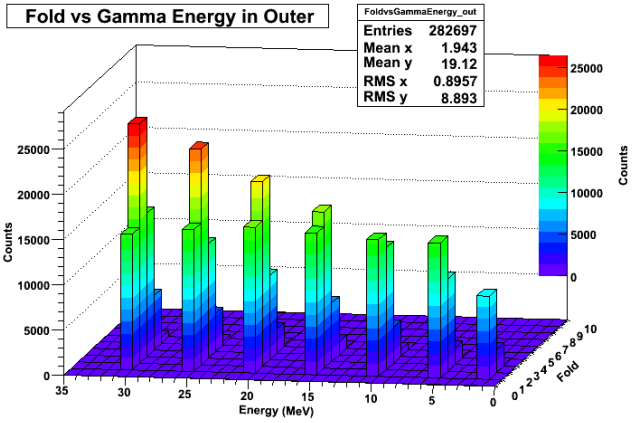

Illustration 45: Fold distribution for the central 6th detector with incident 1,5,10,15,20,25,30MeV gammas in a 4x4 array of 3"x3"x8" CsI crystals

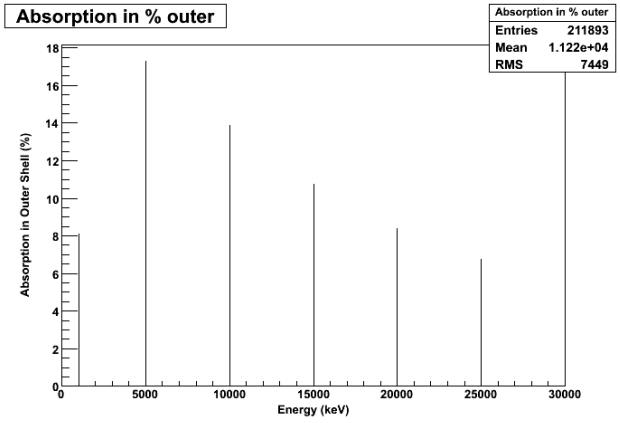

Illustration 46: The percent of absorption of 1,5,10,15,20,25,30MeV gammas in the central 6th detector in a 4x4 array of 3"x3"x8" CsI crystals.

Now, we see that the increase in counts in the outer shell of crystals is roughly the same, an increase of around 2.3% of the total entries, deviating by only 0.5% from the last simulation done with smaller sized crystals. It is now safe to conclude that the boost in efficiency for this configuration is not enough for it to surpass the other arrangement in terms of absorption. Therefore, I maintain that 2" crystals in a 4x4 array would still be the best and most beneficial configuration for PARIS in terms of practical applications. To give a boost to the number of counts in the outer shell (albeit a small one), all simulations will fix the length of CsI at 8" from this point on.

No simulations were conducted by extending the length of CsI to 10” as the increase in the amount of absorption and number of counts is expected not to differ much from previous results due to the increasing distance from the source for the volume of crystal. Since the increase in extending the outer crystal 2 inches from 6 to 8” was only a 2.2-2.3% increase in the amount of absorption, one can assume that any further increase from extending the volume of CsI further will result in negligible gain of absorption. Obviously, no simulations were conducted either for any shorter length than 6” as the number of counts will be reduced significantly, and this will result in a poor practical application of PARIS.

The Addition of Gaps

Previously all the simulations were done with no gap between the crystals, except for the further segmented case where we assumed a gap around each glued crystal of 5mm. This of course is unrealistic as wiring and cooling appliances needed to be fitted. This will no doubt compromise the efficiency of absorption in the $LaBr_3$ and CsI crystals, but how much so? I ran two simulations, one involving a spacing added between the crystals, keeping the two crystal stuck together at one face, and another where all the crystals sides were separated by the same amount of spacing. These tests were conducted investigating the change of absorption efficiency with gap sizes of 5mm and 10mm.

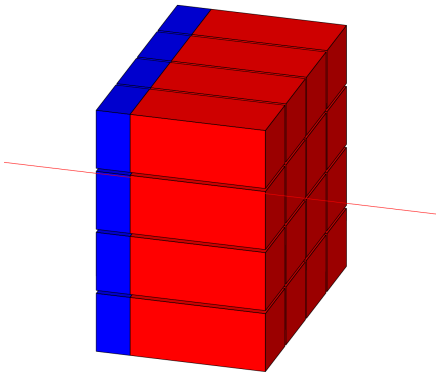

Illustration 47: A model of the set-up which shows a spacing of 5mm between the sides of the crystals, which are glued at one end

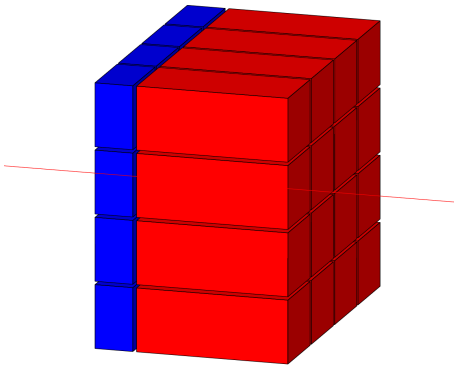

Illustration 48: A model of the set-up which shows a spacing of 5mm around all sides of the crystals

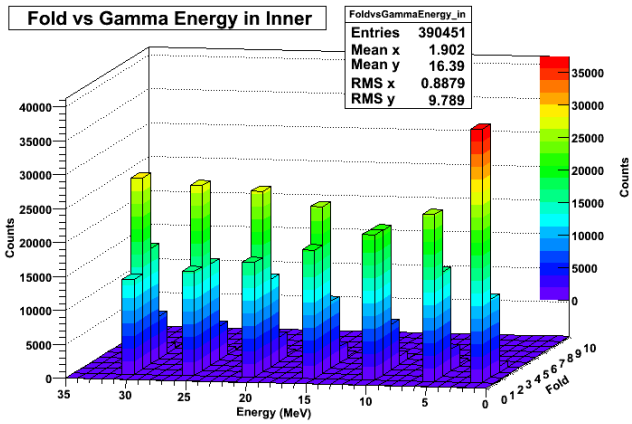

Illustration 49: A fold distribution graph showing the result of multiple energy gammas incident on the inner shell of crystals with 5mm spacing on the sides of the crystals, one face glued to another

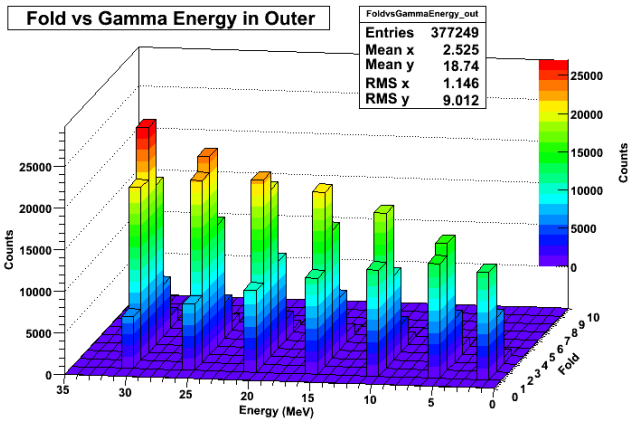

Illustration 50: A fold distribution graph showing the result of multiple energy gammas incident on the outer shell of crystals with 5mm spacing on the sides of the crystals, one face glued to another

There is a reduction in the amount of total absorption by about 18.6% in the inner amount of crystals, and a reduction of 1.2% in the outer shell, almost making the extension of the crystal volume discussed previously obsolete. Instead of 52% of incident 1MeV gammas being absorbed, only 46% seem to deposit their energy with this set-up, all other incident energies experiencea reduction in absorption efficiency of around 2-3% to what wasobserved previously. In the outer absorption there is only a 5.5% drop in the absorption efficiency, with most of the loss in efficiency attributed to the incident 10MeV gamma, all other energies seem to show a rise in absorption efficiency, especially low gammas for which there is a 3% increase in absorption for incident 1MeV gammas.

Now we see what the fold distribution is like where instead of gluing the incident faces of both crystals together, we have a spacing around all sides of the detector.

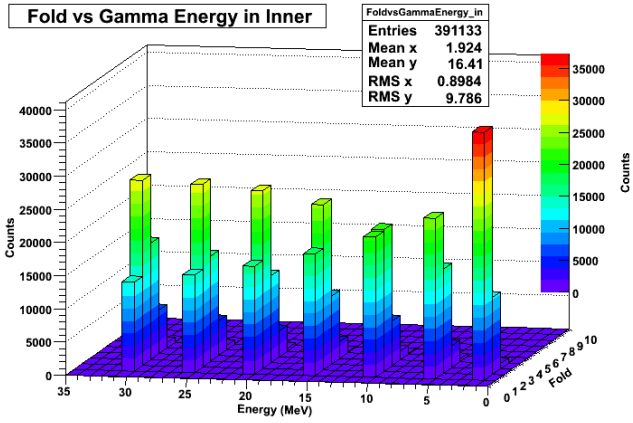

Illustration 51: A fold distribution graph showing the result of multiple energy gammas incident on the inner shell of crystals with 5mm spacing all around the crystals

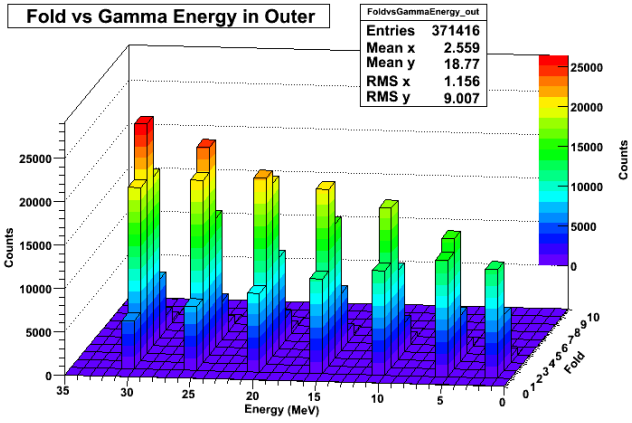

Illustration 52: A fold distribution graph showing the result of multiple energy gammas incident on the outer shell of crystals with 5mm spacing all around the crystals

For the configuration where the spacing is around all the crystals (Illustration 9), we see that there is no major difference with the inner shell of crystals, the absorption remaining close to the same values as the previous simulation. In the outer shell, the difference in total absorption is only a decrease of 0.9% in the total absorption. So, the absorption efficiency doesn't seem to take such a drastic drop with additional spacing behind the $LaBr_3$ crystals, but how big can we make this gap before a noticeably poor efficiency is achieved? I investigated this by adding spacing of 10mm around the sides of the crystals.

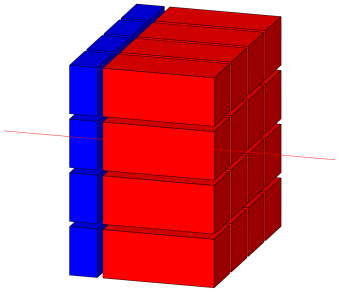

Illustration 53: A model of the set-up which shows a spacing of 10mm between the sides of the crystals, which are glued at one end

One would immediately assume poorer results all around. After simulating what one would see for a 10mm spacing around the crystals, we observe the following distribution in fold in the graphs overleaf. The number of fold is greatly increased with energy deposited in as many as 8 fold! This is similar to what we saw before, although the number of interactions seemed to be contained in around 6 or 7 fold. The absorption efficiency is also poorer, as one might expect. Compared to the other graphs we see a further reduction in efficiency of 33.8% (or 52.4% with no gaps) for the inner shell of crystals. For the outer shell of CsI crystals we see a further reduction of 12.4 % (or 18.8% with no gaps), indicating this gap size is probably too big and thus a limit of 5mm spacing would be justified. Spacing around the detectors gives us less absorption (a marginal amount) than when we glue one face, and thus the latter should be used in following simulations.

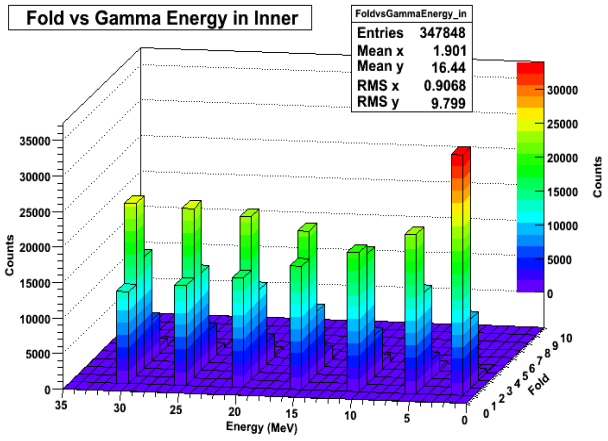

Illustration 54: A fold distribution graph showing the result of multiple energy gammas incident on the inner shell of crystals with 10mm spacing all around the crystals

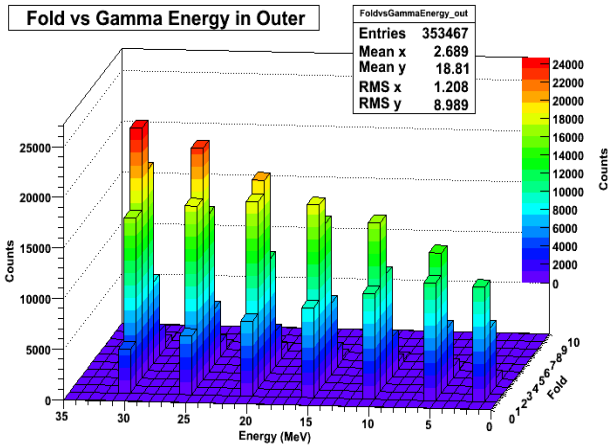

Illustration 55: A fold distribution graph showing the result of multiple energy gammas incident on the outer shell of crystals with 10mm spacing all around the crystals

The overall trend can now be seen in the following graphs which show the absorption efficiencies for different gap sizes with one face glued and gaps around the crystals.

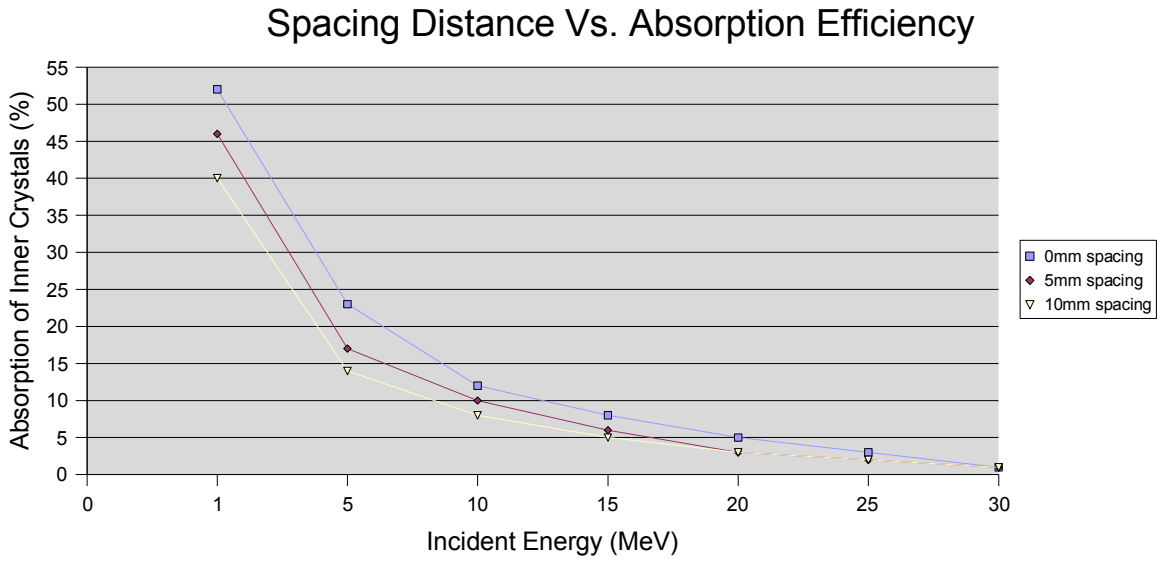

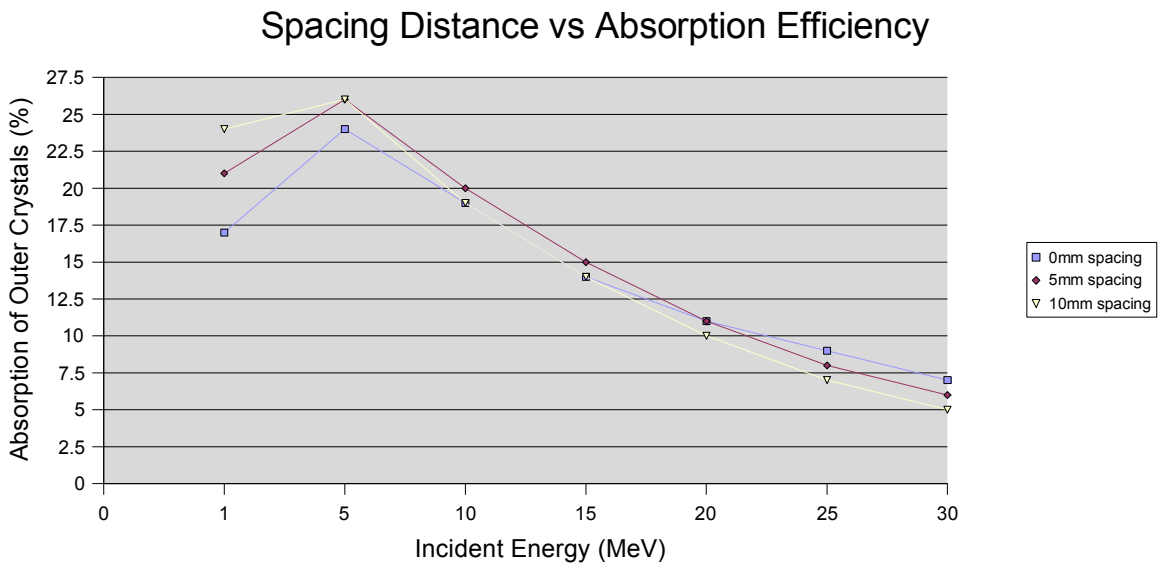

As one can see from the absorption graphs above, there is a decrease in the efficiency when we have an increase in spacing between the inner crystals. However, this effect is the opposite when looking at the efficiency of the outer crystals due to the crystals in the inner shell being more unable to capture gammas and thus allows more interactions in the outer shell.

From now on, the simulations will keep the 5mm gap spacing as it is most realistic and best alternative from the simulations we have seen. Also, we have seen that spacing around all the detectors mean less absorption (although a small amount). Therefore, simulations should be conducted with the Phoswitch set-up where one face is glued to the other crystal, and a gap of 5mm is left around the remaining detector to allow for wiring and cooling apparatus.

Summary

As we have seen there are many different configurations the PARIS detector can take, even with just the cubic design and arrangement!However, I have found through intensive simulation work that the best configuration to use for the modules in the PARIS calorimeter are 2” crystals in a 4x4 array. I then investigated if other methods of segmentation yielded poorer or better results, with the outcome being the former for the simulations conducted using the best array. I also found that extending the length of the outer CsI crystal gave us a negligible result in terms of absorption efficiency and counts. I then finished off by stating that 5mm gaps is the most reasonable solution when incorporating realistic situations into the geometry in terms of additional apparatus. A 4x4 array of crystals results in 96 detectors (Phoswitches) used in the entire array which will result in low granularity. Therefore, more ambitious designs involving larger arrays and more detectors, with the crystal size being kept at 2” as a lower limit from the work seen here, would result in higher granularity. Energy resolution spectra has been produced with this work but is not included in the report, and no simulations have yet been produced with the more ambitious designs, but are currently in the works.